Title
Ice motion of the Patagonian Icefields of South America: 1984–2014

Journal
Geophysical Research Letters, 42(5)

ISSN
0094-8276

Authors
Mouginot, J
Rignot, E

Publication Date
2015-03-16

DOI
10.1002/2014gl062661

AGU PUBLICATIONS

Geophysical Research Letters

RESEARCH LETTER
10.1002/2014GL062661

Key Points:
- First complete velocity mapping of the Patagonian Icefields
- Long-term and seasonal speed changes of major glaciers over the last 30 years
- Redefinition of the drainage boundary of the Patagonian Icefields

Supporting Information:
- Table S2
- Table S1
- Text S1 and Figures S1 to S7

Correspondence to:
J. Mouginot,
jmougino@uci.edu

Citation:
Mouginot, J., and E. Rignot (2015), Ice motion of the Patagonian Icefields of South America: 1984–2014, *Geophys. Res. Lett.*, *42*, 1441–1449, doi:10.1002/2014GL062661.

Received 1 DEC 2014
Accepted 4 FEB 2015
Accepted article online 9 FEB 2015
Published online 9 MAR 2015

Ice motion of the Patagonian Icefields of South America: 1984–2014

J. Mouginot[1] and E. Rignot[1,2]

[1]Department of Earth System Science, University of California, Irvine, California, USA, [2]Jet Propulsion Laboratory, California Institute of Technology, Pasadena, California, USA

Abstract We present the first comprehensive high-resolution mosaic of ice velocity of the Northern (NPI) and Southern Patagonian Icefields (SPI), from multiple synthetic aperture radar and optical data collected between 1984 and 2014. The results reveal that many of the outlet glaciers extend far into the central ice plateaus, which implies that changes in ice dynamics propagate far inside the accumulation area. We report pronounced seasonal to interannual variability of ice motion on Pío XI and Jorge Montt, a doubling in speed of Jorge Montt, a major slow down of O'Higgins, significant fluctuations of Upsala and a deceleration of San Rafael, which illustrate the need for sustained, continuous time series of ice motion to understand the long-term evolution of the rapidly thinning icefields. The velocity product also resolves major ambiguities in glacier drainage in areas of relatively flat topography illustrating the need to combine topography and flow direction to map drainage basins.

1. Introduction

The Northern and Southern Patagonian Icefields (abbreviated NPI and SPI, respectively) are the largest temperate ice masses in the Southern Hemisphere outside of Antarctica [*Aniya et al.*, 1996]. The icefields are losing mass rapidly with the largest contribution to sea level rise per unit area in the world [*Rignot et al.*, 2003; *Chen et al.*, 2007; *Rivera et al.*, 2007; *Glasser et al.*, 2011; *Ivins et al.*, 2011; *Willis et al.*, 2012a, 2012b; *Gardner et al.*, 2013; *Jaber et al.*, 2013]. The NPI is about 4200 km^2 in size, in southern of Chile, around 47°S and 73.5°W [*Aniya*, 1988]. The SPI spreads across the border of Chile and Argentina and is a north-south elongated area about 13,000 km^2 in size between 48.15°S and 51.4°S [*Aniya et al.*, 1996]. The outlet glaciers of NPI are mostly land terminating or calve in proglacial lakes (e.g., San Quintín, Nef, Leones, Reicher, Gualas), with the exception of Glaciar San Rafael which calves into a laguna connected to the ocean via the Río Témpano, a 30 m deep channel. In contrast, most glaciers of SPI calve into ocean waters on the west coast and proglacial lakes in the east.

Knowledge of ice velocity is essential to identify areas of rapid ice discharge, define the origin of ice and the limits of glacier catchments, calculate ice discharge into lakes or the ocean, and compare the results with surface mass balance to estimate the icefield mass balance, or study ice flow dynamics in relation to climate change. Until recently, only partial coverage of ice motion of the Patagonian Icefields has been available [*Naruse et al.*, 1992; *Michel and Rignot*, 1999; *Skvarca et al.*, 2003; *Rivera et al.*, 2007; *Stuefer et al.*, 2007; *Ciappa et al.*, 2010; *Sugiyama et al.*, 2011; *Rivera et al.*, 2012a; *Willis et al.*, 2012a; *Muto and Furuya*, 2013; *Sakakibara et al.*, 2013; *Sakakibara and Sugiyama*, 2014]. The advent of the interferometric synthetic aperture radars (InSAR) provides large-scale, high-resolution coverage of the icefields independent of cloud cover and solar illumination, at a high level of precision [*Rignot*, 1998]. To date, few of these observations have been processed into ice velocity products. Hence, the mapping of ice velocity has been limited to a few glaciers, mostly at low elevation [*Rivera et al.*, 2012a; *Willis et al.*, 2012a; *Muto and Furuya*, 2013].

Here we present a near-complete map of ice velocity of the NPI and SPI assembled from satellite InSAR data acquired between 1994 and 2010 by five instruments, complemented with time series of ice motion derived from Landsat data going back to 1984. We discuss the flow structure of the icefield, temporal variations in ice velocity of major glaciers, and a revision of major glacier catchments and conclude on the impact of ice dynamics on the evolution of the icefields.

2. Data and Methods

We use data collected by five SAR satellites and Landsat managed by four space agencies: (1) NASA's Spaceborne Imaging Radar-C (SIR-C) from Fall 1994, and Landsat satellites from 1984 to the present, (2) the European Space Agency's Earth Remote Sensing satellites (ERS-1 and ERS-2) from winter 1995 to 1996, (3) the Canadian Space Agency's RADARSAT-1 from fall 2004 to Spring 2008, and (4) the Japanese Space Agency's Advanced Land Observation System (ALOS) Phased Array type L-band SAR (PALSAR) for winter 2007 and fall to winter 2010. ERS-1/ERS-2 and RADARSAT-1 operated at the C band frequency (5.6 cm wavelength), ALOS at the L band frequency (24 cm wavelength), and SIR-C simultaneously at C and L bands. The SAR data are processed from raw data to single-look complex format using the GAMMA processor (www.gamma-rs.ch, *Werner et al.* [2001]). Surface ice motion is detected using a speckle tracking algorithm [*Michel and Rignot*, 1999] for SIR-C, ERS (35 day repeat), RADARSAT-1, and ALOS, the interferometric phase of ascending and descending tracks for ERS-1/ERS-2 (1 day repeat) [*Joughin et al.*, 1998], and feature tracking for Landsat. The cross-correlation program for both SAR and optical images is `ampcor` from the Jet Propulsion Laboratory/California Institute of Technology repeat orbit interferometry package (ROI_PAC) [*Rosen et al.*, 2004]. The correlation is performed on subimages of about 350 × 350 m in size and on a regular grid with a spacing of 100 × 100 m. We eliminated pixels for which offsets deviate by more than two units from offsets filtered by a 5 × 5 pixel median filter [*Mouginot et al.*, 2012]. We used a 3 × 3 pixel median filter to remove any remaining false detection. Ice flow vectors are formed assuming surface parallel flow, using the digital elevation model (DEM) from the Shuttle Radar Topography Mission (SRTM) of fall 2000. In reality, ice flow is only parallel to the ice surface at the equilibrium line altitude when the glacier is in steady state, but this is the best approximation that we can use in the absence of multiple-look angles of the glaciers (a minimum of three independent look directions is required to map ice motion in three dimensions). The calibration of the offsets is made using the numerous ice-free rock areas that provide natural targets of zero motion. The horizontal resolution of the velocity measurement is about 300 m and glaciers smaller in size than 500 m may not be fully captured, which we estimate to represent much less than 10% of the total area of the icefields.

The mapping precision of ice motion varies with instrument, location, technique of analysis, repeat cycle, and time period. For each individual track, we estimated the 1 sigma error from the distribution of absolute displacement in ice-free areas (see Table S1 in the supporting information), where motion should be zero. We found that the mean 1 sigma error of ice velocity mapping for ALOS, RADARSAT, ERS, SIR-C, Landsat-4, Landsat-7, and -8 is, respectively, 3.5, 4.7, 17, 21, 52, and 28 m/yr.

The final mosaic combines a total of 180 SAR tracks on a map at 100 m sample spacing (see Table S1 and Figure S7). The Landsat data are not used in the mosaic. Signal coherence is typically low in the interior regions because of the long repeat cycle of RADARSAT-1 (24 days) and ALOS PALSAR (46 days). In these areas, we rely solely on ERS-1/ERS-2 1 day repeat pass interferometry and two tracks from SIR-C with 1 to 4 days repeat. In the presence of multiple tracks, we calculate a weighted average of the velocity with a weight of 1 for year 2004, 2005; 0.2 for years 1996, 2000, 2006, and 2007; and 0.1 for every year before 1996 or after 2007. In this manner, the lower part of the icefields is mostly representative of conditions in 2004–2005. The upper part, where ice speed is low and temporal changes are expected to be less significant, is mainly covered by ERS data from 1996. Overall, the ice motion mosaic is mostly representative of ice surface conditions in year 2004. Care should be exercised if using the complete velocity map for change detection because of the large temporal changes occurring seasonally and annually on some glaciers as discussed later on.

Using the ice flow direction (see Figure S6), we updated the 2007 basins derived by *Davies and Glasser* [2012] and distributed on the Global Land Ice Measurements from Space (GLIMS). The mapping of *Davies and Glasser* [2012] was mainly based on surface slope from the SRTM and Landsat images. Shallow surface slopes are encountered on the broad plateaus of the NPI and the SPI, but also in the drainage of Glaciar Penguin and Glaciar Europa in the central part of the SPI. In these flat areas, ice flow direction is a more reliable indicator of drainage and is used here to update the misplaced ice divides. The divides are manually mapped by following the flow direction or flow lines computed every 300 m from the ice motion map.

3. Results

Figure 1 shows a comprehensive view of ice flow in the NPI and SPI. Surface velocities are available over 4100 km^2 or 97% of NPI (Figure 1a) and 11,300 km^2 or 87% of SPI (Figures 1b and 1c). Ice velocity ranges

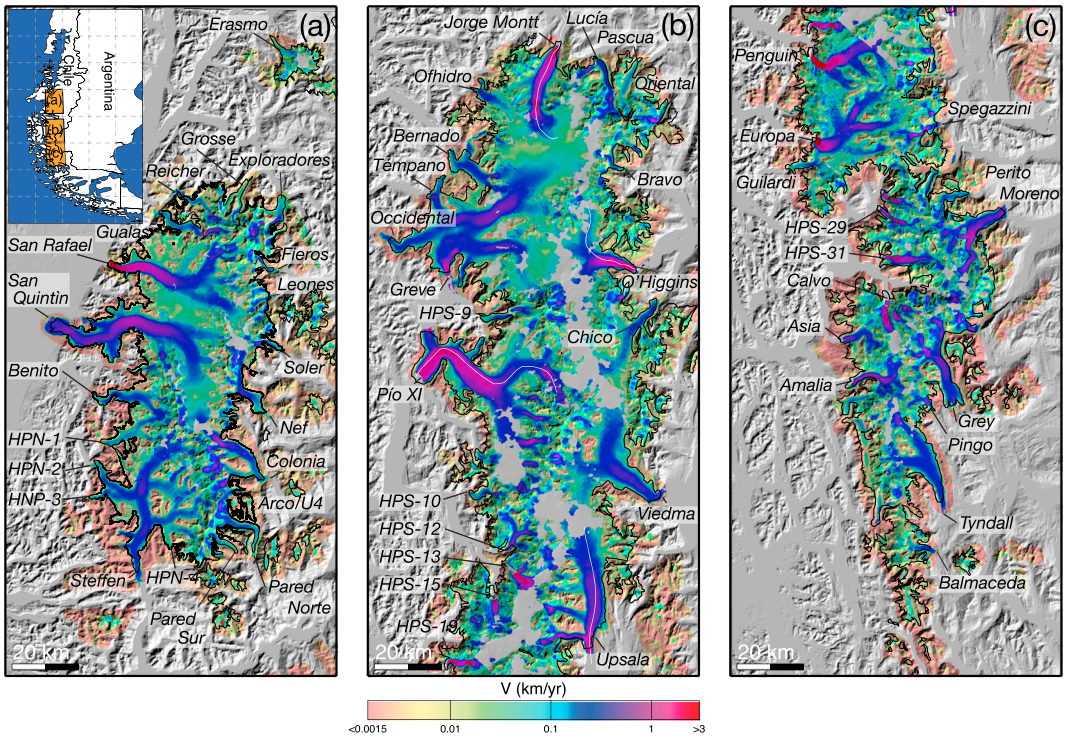

Figure 1. Flow speed of (a) the Northern Patagonia Icefield (NPI), and the (b) northern and (c) southern parts of the Southern Patagonia Icefield (SPI) derived from satellite radar interferometry observations spanning from 1994 to 2014, color coded on a logarithmic scale and overlaid the Shuttle Radar Topography Mapping (SRTM) Digital Elevation Model (DEM) shaded relief. White lines indicate flow lines used in Figure 2. The black line indicates the 2007 external outlines of the icefields [*Davies and Glasser*, 2012].

from a few cm/yr near ice divides to 10 km/yr for the fastest-moving glaciers, i.e., varies by 6 orders magnitude. Large portions of the icefields experience enhanced ice flow (> 200 m/yr) that extends many tens of kilometers into the ice plateaus. In total, more than 40% of the ice domain flows at speeds greater than 100 m/yr. If we assume ice thickness around 700 m on the plateau [*Casassa*, 1987; *Naruse et al.*, 1992; *Rivera and Casassa*, 2002; *Raymond et al.*, 2005; *Zamora et al.*, 2009], ice flow from internal deformation of temperate ice should be less than about 50 m/yr (see SOM), which indicates that large portions of the icefields must be sliding over their beds. Ice flow speeds are generally higher in the west than in the east, which is certainly related to the large west-east gradient in accumulation [*Lenaerts et al.*, 2014], combined with differences in air/ocean temperature on the ocean side (west) versus the air/lake temperature on the lake side (east). The asymmetry in ice speed is, however, less pronounced in the southern part of SPI where drainage basins are typically smaller in size than in the north of the SPI.

3.1. Northern Patagonian Icefield

The fastest glacier of NPI, Glaciar San Rafael, flows at 7.6 km/yr, as measured by SIR-C in 1994, or 21 m/d. It is challenging to measure the flow speed of its terminus with other SAR sensors because their time repeat is too long to maintain signal coherence (e.g., ice moves 1 km in 46 days). This maximum speed is in agreement with recent measurements by *Willis et al.* [2012a] using 7 day repeat Advanced Spaceborne Thermal Emission and Reflection Radiometer (ASTER) data from year 2007. The glacier has been experiencing a retreat of 1.2 km since 1986 (see Figure S1). Over that time period, we detect only slight changes in speed about 10 km from the ice front (see Figure S1). In that region, the glacier speed peaked in 2005, about 15% higher than in 1994, and decreased by about 20% thereafter.

The second largest glacier, Glaciar San Quintìn, is comparable in size to Glaciar San Rafael but terminates in a proglacial lake and reaches its maximum speed about 29 km from the ice front, at about 1.1 km/yr, in the narrowest section of the terminal valley, closest to the equilibrium line altitude (ELA) [*Rivera et al.*, 2007]. Its terminus has been undergoing a steady retreat with decay of its piemont lobe [*Davies and Glasser*, 2012]. As

a result, we find that the surface ice motion near the front of San Quintìn has accelerated from 0.15 km/yr in 1987 to 0.85 km/yr in 2014 (Figure S2).

The two glaciers drain together 37% of the NPI. We observe high flow rates, > 100 m/yr, over more than 90% of the glacier lengths, indicating a rapid transfer of mass from the source of these glaciers to their termini. Glaciar San Rafael's northern branch initiates at the foothill (within 3 km) of Monte San Valentin, the highest peak in the region at 4080 m, while its central branch extends within 7 km of the east side of NPI. An area of slow motion about 2.0 km × 1.6 km is visible in the central plateau, at 46.76°S, 73.5°W, probably because of an unknown subglacial peak. Glaciar San Quintìn's main tributary extends to the central part of NPI at 47.04°S. In the southern part, Glaciar Steffen is the third largest glacier, with a catchment common with HPN-2 and HPN-3, a main tributary to the north at the foothills of Monte Arenales and several tributaries to the east. In the central west, Glaciar Benito and HPN-1 share one tributary. All these glaciers take their source along the Cordón Aisén range and experience fast flow rates.

3.2. Southern Patagonian Icefield

The largest glacier catchments of SPI are those of Glaciares Pío XI, Viedma, O'Higgins, Upsala, Bernado, and Jorge Montt [*Aniya et al.*, 1996]. Only few catchment basins are unmapped (Figure 1), all in the central plateau. Signal coherence is low on the plateau and difficult to maintain if the repeat cycle is more than 5 days. The tandem ERS-1/ERS-2 and SIR-C pairs are the only data that provide ice velocity estimates on the plateau. Even then, it is challenging to find good correlation between pairs; hence, the residual gaps on the upper part of Glaciares O'Higgins, Chico, Upsala, Pío XI, HPS-13, HPS-15, and HPS-19.

In the southern part of SPI (Figure 1), we find some of the fastest-flowing glaciers in the world with velocities up to 10.3 km/yr for Glaciar Penguin (28 m/d), 8.8 km/yr for Glaciar Europa (24 m/d), 6.0 km/yr for HPS-19 (16 m/d), and 5.0 km/yr for HPS-28 (14 m/d) (see Table S2). These glaciers are only surpassed in speed by few glaciers in Greenland [*Rignot and Mouginot*, 2012; *Moon et al.*, 2012; *Joughin et al.*, 2014]. They are all terminating in the Pacific Ocean. Glaciar Jorge Montt, the northernmost glacier of SPI (Figure 1) retreated by 13 km between 1984 and 2014 (*Rivera et al.* [2012b], Figure 2a). Its ice speed more than doubled between winter 1986 and winter 2000, then the glacier slowed down by 30% between 2000 and 2008 and accelerated again by 115% between 2008 and 2014. Overall, the speed 15 km from the 1985 ice front increased from 0.8 km/yr in 1986 to 2.6 km/yr in 2014 (7 m/d). Speed changes propagated at least 30 km from the ice front. We also find during the time period 2000–2010 when we have dense time series of ice velocity that Glaciar Jorge Montt is subject to strong seasonal cycles. Its ice speed fluctuates within 1 year by ±0.2 km/yr or 13%, and the seasonal maximum is reached around mid-November (Figure 2a).

Glaciar Pío XI, formally known as Brügen Glacier, also marine terminating, is the largest glacier catchment of SPI and exhibits some of the largest long-term and seasonal fluctuations in flow speed (Figure 2b). Its seasonal cycle has an amplitude of 0.4 km/yr about 15 km from its southern ice front, which is the largest in Patagonia, with a peak speed in mid-October about 40% higher than its annual mean. In contrast, the northern branch of the glacier does not experience significant seasonal variability. The long-term fluctuation in speed is also significant. The annual mean speed 15 km from the ice front increased from 2 to 2.5 km/yr between 1986 and 2001, decreased until 2009–2010 to 1.5 km/yr and remained constant ever since. The largest speed changes are observed near the ice front, with 2.5 km/yr in 1986, more than 6 km/yr in 2000, 3 km/yr between 2004 and 2006 and an abrupt change after 2006 with a mean flow rate of only 0.5 km/yr. Interestingly, the northern branch of the glacier displays an opposite trend (see Figure S3): slowdown between 1986 and 2011 from 1.4 km/yr to 0.2 km/yr, then acceleration to 1 km/yr in 2014. This suggests that ice discharge oscillates between the northern and southern branches of the glacier.

Glaciar O'Higgins retreated considerably in 1945–1985 passed an overdeepening more than 800 m deep in Lago O'Higgins [*Schaefer et al.*, 2011], the deepest lake in South America [*Casassa et al.*, 1997]. Between 1984 and 2014, the terminus retreated by only 1 km (Figure 2c). Its speed 3 km from the ice front decreased steadily from 4 km/yr to 2 km/yr between 1984 and 2014, or reduced by half (Figure 2c). Although the time series of data is limited on Glaciar O'Higgins, it appears that the seasonal fluctuations in speed are not significant, or less than 3% of the mean annual speed.

Ice velocity on Glaciar Upsala doubled from 1985 to 2001, then decreased between 2001 and 2005 by 20% to increase again by 50% between 2005 and 2010 before decreasing again until 2014 (Figure 2d). The ice flow acceleration coincides with a rapid retreat of its terminus (Figure 2d). The flow rate decelerated during

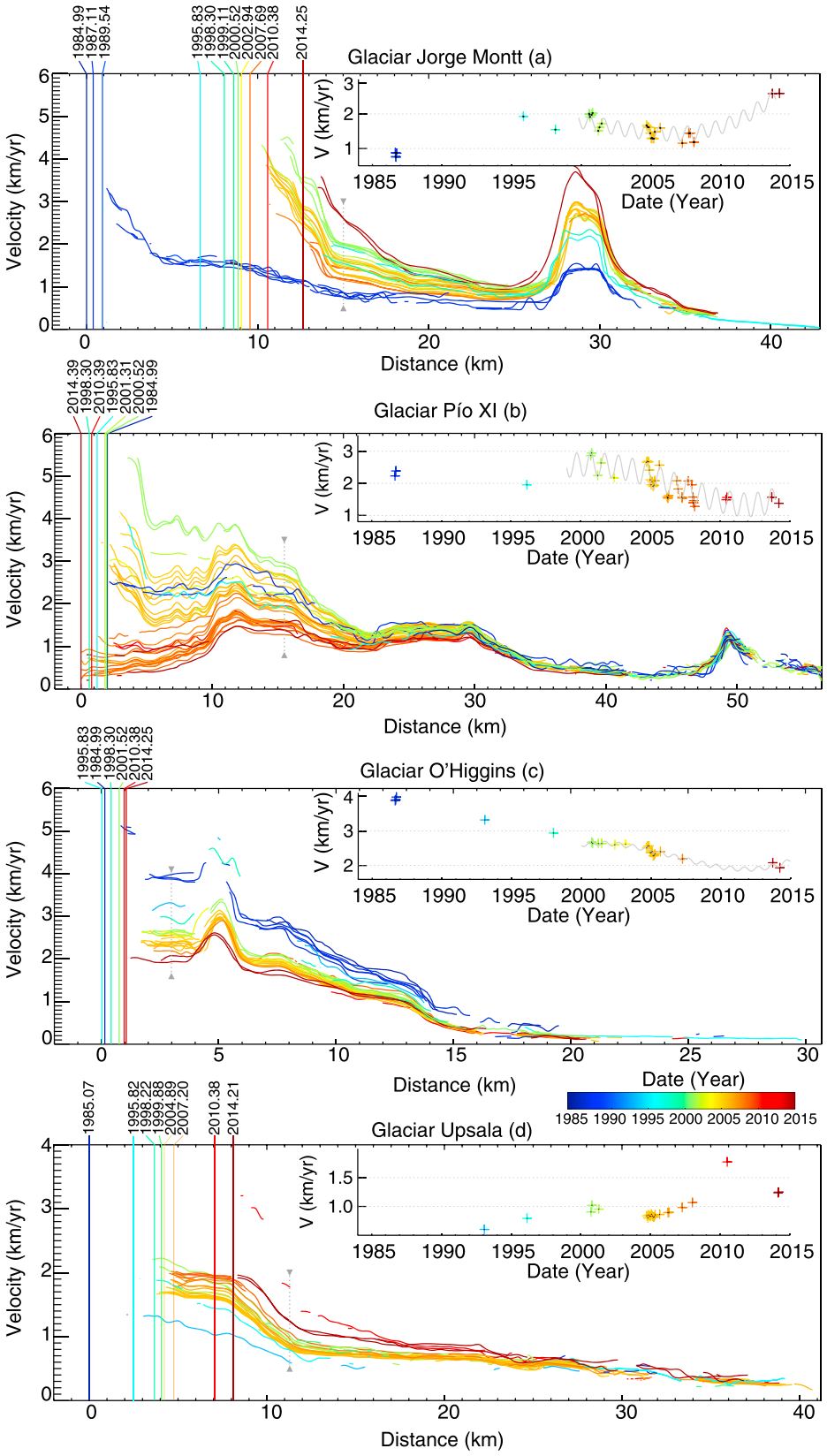

Figure 2. Flow speed along the flow lines in Figure 1 color coded from 1984 (blue) to 2014 (red). Vertical lines indicate the position of the terminus with time. The inset displays the speed versus time at the location indicated by the grey dashed on the main plot. To show the seasonal fluctuations, we fit the flow speed with a sinusoid function (grey line).

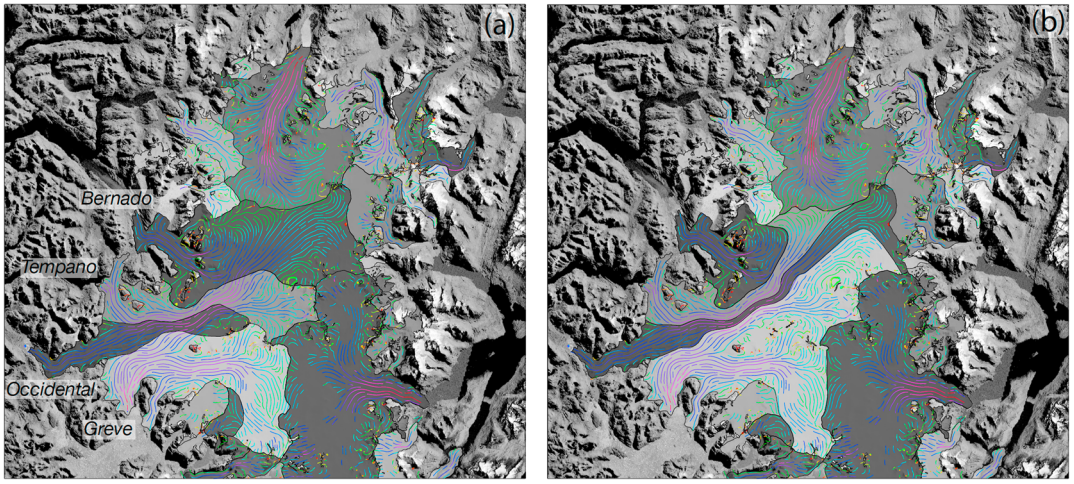

Figure 3. Drainage basins of the northern part of SPI from (a) *Davies and Glasser* [2012] and (b) based on the ice motion map from this study. Flow lines derived herein are shown on both panels color coded as in Figure 1. A Landsat 7 mosaic from 2001 to 2003 is used for the background.

periods of slower retreat. Glaciar Upsala does not seem to exhibit seasonal variation in speed during the time period 2000–2010.

In the northern part of SPI, we find major differences in flow drainage compared to prior studies [*Davies and Glasser*, 2012; *Rivera et al.*, 2012b; *Casassa et al.*, 2014] that did not benefit from ice flow information (Figure 3). As the result of the new information on flow direction, the basins of Glaciar Bernado, Témpano, Occidental, and Greve are largely redefined, with areas updated from 522, 322, 203, and 435 km^2, respectively, to 193, 223, 292, and 759 km^2. The catchment of Glaciar Bernado is much smaller than in prior inventories, and most of the ice from the central plateau is drained by Glaciar Occidental and Greve which together drain the second largest basin in Patagonia. Témpano and Occidental flow parallel to each other until they split into different terminal valleys. Together they form the sixth largest drainage in SPI. Greve basin (759 km^2) is nearly twice larger than previously thought and comparable in size to Upsala or Viedma (874 and 875 km^2).

The divide between Glaciar Europa and Penguin is also revised. The basin of Glaciar Europa was underestimated from surface topography alone (Table S2, Figure S5). In the NPI, the drainage boundary between Glaciar San Rafael and San Quintín is more firmly defined and differs from that inferred from GLIMS (Figure S4), with the result that the two basins are now nearly equal in size.

4. Discussion

The complete map of ice motion of NPI and SPI reveals the extent of tributary flow and the complete range of ice motion across the entire icefields. Many of these outlet glaciers are seen to extend far into the ice plateaus, which was not known previously. This implies that a dominant part of the evolution of the ice plateau is controlled by ice dynamics rather than by surface mass balance processes alone. This probably explains why ice thinning is detected well above the ELA of these glaciers, and in some cases to the flanks of ice divides [*Rignot et al.*, 2003; *Willis et al.*, 2012a, 2012b; *Jaber et al.*, 2013]. We interpret these zones of thinning as the result of draw down of the plateaus by the glaciers, not from a decrease in snow accumulation. Observed changes in ice elevation on the plateau of NPI using altimetry data or differencing of DEMs should not be interpreted assuming that the signal is dominated by changes in snowfall because these areas are significantly influenced by the flow of Glaciar San Rafael and San Quintín, which is time dependent. In addition, ice flow speed well above 100 m/yr (see Figure 1) indicates sliding of ice on the glacier bed over a large share of the accumulation area of NPI and SPI. This is contrary to the traditional view that internal deformation dominates flow in the interior regions and fast sliding only dominates along the periphery. In Patagonia, we observe that the vast majority of the icefields must be influenced by sliding. This also implies that changes in flow speed initiated near the frontal regions will propagate rapidly inland and affect the entire icefields, not just the terminal valleys.

The long period of survey and the dense time sequence between 2000 and 2008 shown here highlights the strong seasonal variability of a number of major Patagonian glaciers, which was not fully captured in previous long records such as *Sakakibara and Sugiyama* [2014]. The most significant variability is recorded on Glaciar Pío XI, along with an asynchronous behavior in speed of its northern and southern branches. The differing behavior of the lake and tidewater branches implies that the flow of ice is, alternatively, diverted toward one or the other. Interestingly, the changes in flow direction do not affect the upper part of the glacier. This glacier is also unique in its proximity to an active volcano, Mount Lautaro, which maintains high levels of geothermal heating and therefore basal melt water production, which has been suggested to explain its surge-type nature [*Rivera et al.*, 1997]. We conjecture that the fluctuations in speed of its termini are associated with the continuing adjustment of the frontal regions to its new glacial maximum since the 1980s. The large fluctuations in speed of the southern ice front may also reflect seasonal variations in ice melting into the ocean, whereas the northern branch ends into a proglacial lake. Freshwater lake, with a maximum temperature at the glacier base of +4°C, driven by the density maximum of freshwater at that temperature, should not vary significantly during the year.

Glaciar Jorge Montt, a major tidewater glacier of the SPI, has experienced large phases of acceleration and deceleration over the last 25 years along with a fast retreat and spectacular rate of ice thinning since 1975 [*Rignot et al.*, 2003; *Rivera et al.*, 2012b; *Sakakibara and Sugiyama*, 2014]. The acceleration phases (1985–2001 and 2009 to the present) occurred when the terminus retreated passed an overdeepening of the ice fjord [*Schaefer et al.*, 2011], similar to Glaciar O'Higgins in 1945–1985; in contrast, the retreat stopped and the glacier decelerated (2001–2009) as the ice front retreated toward a bump in bed topography at the head of the fjord [*Rivera et al.*, 2012b]. Fast flow is detected to the flanks of the ice divide with Glaciar Témpano, implying that the entire drainage system is currently experiencing a draw down to sea. Glaciar Jorge Montt, a marine-terminating glacier also exhibits large seasonal fluctuations which we tentatively attribute to seasonal variations in ocean thermal forcing at the ice front. These seasonal variations in ocean temperature at the ice front, combined with seasonal variations in the amount of subglacial discharge at the ice front, will modulate the rate of subaqueous melting of ice at the glacier front [*Xu et al.*, 2013].

The complete map of ice velocity is of critical importance to interpret changes in ice elevation measured by satellites or airborne instruments. It highlights that many parts of the central plateaus are dominated by ice dynamics because they are underlaid by a fast moving stream of ice. The revision of a number of drainage basins is critical to the estimation of the mass balance of each individual glacier by comparing ice discharge along the periphery with surface mass balance in the interior. In the case of Glaciar Greve for instance, it would not be possible to conclude on its state of mass balance based on earlier inventories.

Our results bring forward the need for continuous, dense, long-term observations of the glaciers—instead of annual time series—in order to better characterize the evolution of Patagonia glaciers, better capture the physics of the glaciers under seasonal forcing and long-term climate change. To complete the mapping of ice velocity and extend it in time, short-time repeat cycles are critical due to the high level of surface weathering of the icefields and the high rates of flow deformation. At present, only the Agencia Spaziale Italiana's COSMO-Skymed (1 day repeat) [*Ciappa et al.*, 2010] and the Japanese Space Agency's ALOS-2/PALSAR-2 (14 day repeat) could provide the data necessary to monitor the Patagonia Icefields entirely, with no data gaps, from the high mountains to the front of the glaciers, but access to these data has remained limited. In the future, NASA and Indian Space Research Organization (ISRO) SAR (NISAR) 8 day repeat mission operating at L band will likely provide the best source of observations of this critical part of the southern hemisphere where glacier changes are rapid and the contribution to sea level per unit area is the largest in the world. In the meantime, snapshots of ice velocity should be interpreted with caution, especially in the case of marine-terminating glaciers exhibiting significant seasonal to interannual fluctuations which may mask the long-term history of the glaciers.

5. Conclusions

Using InSAR data from multiple platforms and over different time periods, we present the first complete map of ice velocity of NPI and SPI, along with extensive time series of ice velocity of their major outlet glaciers. The results help redefine the drainage boundaries of major glaciers and emphasize the importance of ice flow dynamics on the evolution of the entire icefields. These glaciers are characterized by the highest flow rates in the world, in addition to what was already known to be the highest precipitation rates in the

world, record rates of thinning and retreat. This is a region of rapid turnover of mass and high rates of mass loss per unit area, which is very important to study. The ice motion map reveals that the glaciers have a more significant and widespread influence on ice elevation changes than previously thought because their zone of fast flow extends far into the central ice plateaus, and in many cases to the flanks of the mountains where they originate. In agreement with *Sakakibara and Sugiyama* [2014], this implies that changes in elevation of the ice plateaus are not dominated by surface mass balance processes and in some areas may, in fact, be dominated by ice dynamics. Sustained and continued observations of these regions are therefore essential to better understand the complex interplay between glacier mass balance and climate change in Patagonia.

Acknowledgments
This work was performed at the University of California, Irvine, and at the Jet Propulsion Laboratory, California Institute of Technology, under a grant from the National Aeronautics and Space Administration. The authors gratefully acknowledge the European Space Agency, the Canadian Space Agency, the Japan Aerospace Exploration Agency, and the National Aeronautics, United States Geological Survey, and Space Administration for the use of ERS-1 and ERS-2, RADARSAT-1, ALOS PALSAR, SIR-C, and Landsat data.

The Editor thanks three anonymous reviewers for their assistance in evaluating this paper.

References

Aniya, M. (1988), Glacier Inventory For The Northern patagonia icefield, Chile, and variations 1944/45 to 1985/86, *Arct. Alp. Res.*, *20*, 179–187.

Aniya, M., H. Sato, R. Naruse, P. Skvarca, and G. Casassa (1996), The use of satellite and airborne imagery to inventory outlet glaciers of the southern Patagonia Icefield, South America, *Photogramm. Eng. Remote Sens.*, *62*, 1361–1369.

Casassa, G. (1987), Ice thickness deduced from gravity anomalies on Soler Glacier, Nef Glacier and the Northern Patagonia Icefield, *Bull. Glaciol. Res.*, *4*, 43–57.

Casassa, G., H. Brecher, A. Rivera, and M. Aniya (1997), A century-long recession record of Glaciar O'Higgins, Chilean Patagonia, *Ann. Glaciol.*, *24*, 106–110, International Symposium on Changing Glaciers, Fjaerland, Norway, 24–27 June 1996.

Casassa, G., J. L. Rodríguez, and T. Loriaux (2014), *A New Glacier Inventory for the Southern Patagonia Icefield and Areal Changes 1986-2000, Springer Prax. Books*, Springer, Berlin.

Chen, J. L., C. R. Wilson, B. D. Tapley, D. D. Blankenship, and E. R. Ivins (2007), Patagonia Icefield melting observed by Gravity Recovery And Climate Experiment (GRACE), *Geophys. Res. Lett.*, *34*, L22501, doi:10.1029/2007GL031871.

Ciappa, A., L. Pietranera, and F. Battazza (2010), Perito Moreno Glacier (Argentina) flow estimation by COSMO SkyMed sequence of high-resolution sar-x imagery, *Remote Sens. Environ.*, *114*, 2088–2096.

Davies, B. J., and N. F. Glasser (2012), Accelerating shrinkage of Patagonian glaciers from the Little Ice Age (similar to AD 1870) to 2011, *J. Glaciol.*, *58*, 1063–1084.

Gardner, A. S., et al. (2013), A reconciled estimate of glacier contributions to sea level rise: 2003 to 2009, *Science*, *340*, 852–857.

Glasser, N. F., S. Harrison, K. N. Jansson, K. Anderson, and A. Cowley (2011), Global sea-level contribution from the Patagonian Icefields since the little ice age maximum, *Nat. Geosci.*, *4*, 303–307.

Ivins, E. R., M. M. Watkins, D.-N. Yuan, R. Dietrich, G. Casassa, and A. Ruelke (2011), On-land ice loss and glacial isostatic adjustment at the Drake Passage: 2003–2009, *J. Geophys. Res.*, *116*, B02403, doi:10.1029/2010JB007607.

Jaber, W., D. Floricioiu, H. Rott, and M. Eineder (2013), Surface elevation changes of glaciers derived from SRTM and Tandem-X DEM differences, in *IEEE Int. Geosci. Remote Sens. Symp. (IGARSS)*, pp. 1893–1896, IEEE, Melbourne, Australia, 21–26 July.

Joughin, I., B. E. Smith, D. E. Shean, and D. Floricioiu (2014), Brief communication: Further summer speedup of Jakobshavn Isbræ, *Cryosphere*, *8*, 209–214.

Joughin, I. R., R. Kwok, and M. A. Fahnestock (1998), Interferometric estimation of three-dimensional ice-flow using ascending and descending passes, *IEEE Trans. Geosci. Remote Sens.*, *36*, 25–37.

Lenaerts, J. T. M., M. R. van den Broeke, J. M. van Wessem, W. J. van de Berg, E. van Meijgaard, L. H. van Ulft, and M. Schaefer (2014), Extreme precipitation and climate gradients in patagonia revealed by high-resolution regional atmospheric climate modeling, *J. Clim.*, *27*, 4607–4621.

Michel, R., and E. Rignot (1999), Flow of Glaciar Moreno, Argentina, from repeat-pass shuttle imaging radar images: Comparison of the phase correlation method with radar interferometry, *J. Glaciol.*, *45*, 93–100.

Moon, T., I. Joughin, B. Smith, and I. Howat (2012), 21st-century evolution of Greenland outlet glacier velocities, *Science*, *336*, 576–578.

Mouginot, J., B. Scheuchl, and E. Rignot (2012), Mapping of ice motion in Antarctica using synthetic-aperture radar data, *Remote Sens.*, *4*, 2753–2767.

Muto, M., and M. Furuya (2013), Surface velocities and ice-front positions of eight major glaciers in the southern Patagonian Ice Field, South America, from 2002 to 2011, *Remote Sens. Environ.*, *139*, 50–59.

Naruse, R., H. Fukami, and M. Aniya (1992), Short-term variations in flow velocity of glaciar soler, Patagonia, Chile, *J. Glaciol.*, *38*, 152–156.

Raymond, C., T. A. Neumann, E. Rignot, K. Echelmeyer, A. Rivera, and G. Casassa (2005), Retreat of Glaciar Tyndall, Patagonia, over the last half-century, *J. Glaciol.*, *51*, 239–247.

Rignot, E. (1998), Radar interferometry detection of hinge-line migration on rutford ice stream and carlson inlet, Antarctica, *Ann. Glaciol.*, *27*, 25–32.

Rignot, E., and J. Mouginot (2012), Ice flow in Greenland for the international polar year 2008–2009, *Geophys. Res. Lett.*, *39*, L11501, doi:10.1029/2012GL051634.

Rignot, E., A. Rivera, and G. Casassa (2003), Contribution of the patagonia icefields of south America to sea level rise, *Science*, *302*, 434–437.

Rivera, A., and G. Casassa (2002), Ice thickness measurements on the southern Patagonia Icefield, in *The Patagonian Icefields, Series of the Centro de Estudios Científicos*, edited by G. Casassa, F. Sepúlveda, and R. Sinclair, pp. 101–115, Springer, New York.

Rivera, A., J. Aravena, and G. Casassa (1997), Recent fluctuations of Glaciar Pio XI, Pagagonia: Discussion of a glacial surge hypothesis, *Mt Res. Dev.*, *17*, 309–322.

Rivera, A., T. Benham, G. Casassa, J. Bamber, and J. A. Dowdeswell (2007), Ice elevation and areal changes of glaciers from the Northern Patagonia Icefield, Chile, *Global Planet. Change*, *59*, 126–137.

Rivera, A., J. Corripio, C. Bravo, and S. Cisternas (2012a), Glaciar Jorge Montt (Chilean Patagonia) dynamics derived from photos obtained by fixed cameras and satellite image feature tracking, *Ann. Glaciol.*, *53*, 147–155.

Rivera, A., M. Koppes, C. Bravo, and J. C. Aravena (2012b), Little Ice Age advance and retreat of Glaciar Jorge Montt, Chilean Patagonia, *Clim. Past*, *8*, 403–414.

Rosen, P. A., S. Hensley, G. Peltzer, and M. Simons (2004), Updated repeat orbit interferometry package released, *Eos Trans. AGU*, *85*, 47.

Sakakibara, D., and S. Sugiyama (2014), Ice-front variations and speed changes of calving glaciers in the Southern Patagonia icefield from 1984 to 2011, *J. Geophys. Res. Earth Surf.*, *119*, 2541–2554.

Sakakibara, D., S. Sugiyama, T. Sawagaki, S. Marinsek, and P. Skvarca (2013), Rapid retreat, acceleration and thinning of Glaciar Upsala, Southern Patagonia Icefield, initiated in 2008, *Ann. Glaciol.*, *54*, 131–138.

Schaefer, M., G. Casassa, and T. Loriaux (2011), Simulating the retreat of the freshwater calving glacier O'Higgins using a flow line model, Geophysical Research Abstracts EGU2011-12379 Presented at EGU General Assembly.

Skvarca, P., B. Raup, and H. De Angelis (2003), Recent behaviour of Glaciar Upsala, a fast-flowing calving glacier in Lago Argentino, Southern Patagonia, *Ann. Glaciol.*, *36*, 184–188.

Stuefer, M., H. Rott, and P. Skvarca (2007), Glaciar perito moreno, patagonia: Climate sensitivities and glacier characteristics preceding the 2003/04 and 2005/06 damming events, *J. Glaciol.*, *53*, 3–16.

Sugiyama, S., P. Skvarca, N. Naito, H. Enomoto, S. Tsutaki, K. Tone, S. Marinsek, and M. Aniya (2011), Ice speed of a calving glacier modulated by small fluctuations in basal water pressure, *Nat. Geosci.*, *4*, 597–600.

Werner, C., U. Wegmüller, T. Strozzi, and A. Wiesmann (2001), Gamma sar and interferometric processing software, in *Proceedings of ERS-ENVISAT Symposium*, edited by H. Sawaya-Lacoste, Eur. Space Agency Publ. Div., Gothenburg, Sweden, 15–20 Oct. 2000.

Willis, M. J., A. K. Melkonian, M. E. Pritchard, and J. M. Ramage (2012a), Ice loss rates at the Northern Patagonian Icefield derived using a decade of satellite remote sensing, *Remote Sens. Environ.*, *117*, 184–198, remote Sensing of Urban Environments.

Willis, M. J., A. K. Melkonian, M. E. Pritchard, and A. Rivera (2012b), Ice loss from the Southern Patagonian Ice Field, South America, between 2000 and 2012, *Geophys. Res. Lett.*, *39*, L17501, doi:10.1029/2012GL053136.

Xu, Y., E. Rignot, I. Fenty, D. Menemenlis, and M. M. Flexas (2013), Subaqueous melting of store glacier, west Greenland from three-dimensional, high-resolution numerical modeling and ocean observations, *Geophys. Res. Lett.*, *40*, 4648–4653, doi:10.1002/grl.50825.

Zamora, R., D. Ulloa, G. Garcia, R. Mella, J. Uribe, J. Wendt, A. Rivera, G. Gacitua, and G. Casassa (2009), Airborne radar sounder for temperate ice: Initial results from patagonia, *J. Glaciol.*, *55*, 507–512.